Egypt. J. Chem. **Vol. 66**, No. 10 pp. 179 - 189 (2023)

Egyptian Journal of Chemistry

http://ejchem.journals.ekb.eg/

Green Synthesis of Magnesium Oxide Nanoparticles Using Probiotic Strain *Lactobacillus Gasseri* and Their Activity against Fungal Strains Isolated From Historical Manuscripts

Gomaa Abdel-Maksoud[a,*], Mahmoud Abdel-Nasser[b], Saad El-Din Hassan[c], Ahmed M. Eid[c], Aya Abdel-Nasser[d], AmrFouda[c,*]

[a]*Conservation Department, Faculty of Archaeology, Cairo University, Giza 12613, Egypt*
[b]*Department of Manuscripts Conservation, Al-Azhar Al-Sharif Library, Cairo 11511, Egypt*
[c]*Department of Botany and Microbiology, Faculty of Science, Al-Azhar University, Nasr City, Cairo 11884, Egypt*
[d]*Food Toxicology and Contaminants Department, National Research Centre, Giza 12622, Egypt*

Abstract

Herein, a cheap, environmentally friendly, rapid, biocompatible, and reproducible green approach was used to synthesize magnesium oxide nanoparticles (MgO-NPs) by harnessing metabolites of probiotic bacteria *Lactobacillus gasseri*. The bacterial-mediated green synthesis of MgO-NPs was characterized by color change, UV-vis spectroscopy, transmission electron microscopy, energy dispersive X-ray, X-ray diffraction, and Fourier transform infrared spectroscopy. Data showed that the color of the cell-free filtrate was changed from colorless to white after mixing with metal precursor and exhibited maximum Surface Plasmon Resonance at 240 nm that confirm the successful formation of MgO-NPs. Moreover, the green synthesized MgO-NPs have a spherical shape with sizes in the ranges of 1–10 nm and are characterized by crystalline nature. The main components of the prepared sample were Mg and O with weight percentages of 42.3 and 36.92% and atomic percentages of 39.07 and 38.7% respectively. The biosynthesized MgO-NPs showed a high inhibitory effect compared to crude extract of probiotic bacteria stain, *L. gasseri* against ten fungal strains (*Aspergillususstus* AM4, *Penicilliumcitrinum* AM5, *Penicilliumchrysogenum* AM11, *A. terreus* AM12, *P. citrinum* AM13, *P. citrinum* AZ8, *P. citrinum* AZ9, *A. niger*AZ11, *P. chrysogenum* AZ12, and *P. chrysogenum* AZ13) which isolated from deteriorated historical paper in a dose-dependent manner. The MIC values of synthesized MgO-NPs were 50–100 µg mL^{-1} with a zone of inhibition of 12.3 ± 0.6–16.3 ± 0.6 mm based on fungal strain.

Keywords: Manuscripts, biodeterioration, biosynthesis, probiotic, *Lactobacillus* spp.,MgO-NPs, antifungal.

1. Introduction

Fungi play a crucial role in the biodeterioration of historical materials such as documents, books, manuscripts, and leather [1-4]. These activities could be attributed to the efficacy of fungal strains to produce various extracellular enzymes that leads to decomposition and weakness of mechanical properties of the materials [5-7]. The efficacy of fungal strains to colonized and deteriorate the historical objects are depending on their secondary metabolites which varied according to fungal species [8, 9]. The most common fungal strains isolated from deteriorated objectswere*Aspergillusniger, A. flavus, A. terreus, A. ochraceous, A. carbonarius, A. fischeri, A. fumigatus, A. tamarii, Eurotiumchevalieri, Cladosporiumcladosporioides, Fusariumpoae, Wallemiasebi , Penicilliumnotatum, P. oxalicum, P. rubrum, and Aletrnariaalternata*[10-15].On the other hand, Airborne fungal spores in storage rooms of museums and libraries can well reach levels of more than 8000/m^3, and their ability to cause systemic infections in humans and seriously threaten the health [16-18]**.**

In a recent study, different fungal strains identified as *Aspergillusdelicatus, A. niger, A. flavus, A. parasiticus, A. oryzae, Penicilliumdigitatum, P. oxalicum, P. expansum, Paecilomyces*sp. and

*Corresponding author e-mail: gomaa2014@cu.edu.eg (Gomaa Abdel-Maksoud), amr_fh83@azhar.edu.eg(AmrFouda)
EJCHEM use only: Received date 10 December 2022; revised date 31 January 2023; accepted date 12 February 2023
DOI: 10.21608/EJCHEM.2023.179933.7297

*Cladosporium*sp. were isolated from deteriorated objects and characterized by their efficacy to producing various hydrolytic enzymes including gelatinase, pectinase, protease, and cellulase[11]. Among 15 fungal strains isolated from high deteriorated historical manuscript dated back to 17th century, *P. chrysogenum* F9 was selected as the most deteriorated fungal strain based on high cellulolytic activity [19].

Recently, metal and metal oxide nanoparticles have been used to control the growth of fungal strains due to unique properties [20, 21]. There are several methods such as chemical, physical, and biological methods were used to fabricate nanoparticles [22, 23]. Researchers are concerned with those synthesized by biological approaches due to it is eco-friendly, rapid, and cost-effective treatment to preserve cultural heritage from microbial deterioration [24, 25].

Magnesium oxide nanoparticles (MgO NPs) have received significant attention as antimicrobial agents in recent years due to their high stability and low cost based on their preparation from economical precursors, corrosion resistance, and high resistance to environmental factors [26, 27]. The mechanism of antimicrobial activity of MgO NPs has been attributed to the production of Reactive Oxygen Species (ROS), which induce oxidative stress and lipid peroxidation in microbes [28].

Lactobacillus Spp. Gram - positive germs are combined into the food industry such as probiotics and nutritional supplements because they are beneficial to humans and enjoy their ability to produce antimicrobial compounds such as protease antibiotics, lipopeptides, and bacteriocin[29]. *Lactobacillus gasseri* is tolerance of acids and produces bacteriosin to reduce pathogenic microorganisms reduces fatty tissue inflammation and utilized for green synthesis of highly stable nanomaterials as a green approach [30].

The main hypothesis of the current study is investigating the efficacy of green synthesized MgO-NPs to inhibit the growth of different fungal strains isolated from highly deteriorated historical manuscripts. To achieve this hypothesis, MgO-NPs were synthesized by harnessing the metabolites of *Lacobacillusgasseri*LA39 and characterized by UV-vis spectroscopy, Fourier Transform Infrared Spectroscopy (FT-IR), X-ray Diffraction (XRD), Transmission Electron Microscope (TEM), and Energy Dispersive X-Ray (EDX) analysis. Moreover, the efficacy of green synthesized MgO-NPs to inhibit the growth of different fungal strains isolated from highly deteriorated historical manuscripts was investigated.

2. Material and Methods

2.1. Probiotic strain

MgO-NPs were fabricated using cell-free filtrate of *Lactobacillus gasseri* LA39. This probiotic strain was kindly obtained from Dr. T. Saito, Faculty of Biological Resource Science, Tohoku University, Japan.

2.2. Biosynthesis of MgO-NPs using *L. gasseri*

The probiotic strain, *L. gasseri* was cultivated in 100 mL of MRS broth media (Ready-prepared, Merck, Germany) followed by incubation at 35±2°C for 24 h. At the end of the incubation period, the inoculated MRS media was centrifuged at 10000 rpm to collect the cells which were resuspended in 100 mL distilled H_2O for 24 h. followed by centrifuging at 1000 rpm for 15 min to collect the cell-free filtrate (CFF) which is used for biosynthesis of MgO-NPs as follows: 77 mg of Mg $(NO_3)_2.6H_2O$ as a precursor was dissolved in 10 mL dis. H_2O and added to 90 mL of collected CFF to get a final concentration of 3 mM. The previous mixture was added to the magnetic stirrer for 1 h at 50°C and adjusted pH at 8 using 1N NaOH which was added drop wise. The transformation of the color of CFF from colorless to white precipitate indicates the formation of MgO-NPs. The mixture was incubated for 24 h to confirm the complete reduction of the precursor. Post 24h., the solution was centrifuged at 10000 rpm for 15 min. The supernatant was carefully discarded, whereas, the white precipitate was collected, and washed thrice with dis. H_2O, and calcinated at 300°C to convert the product from hydroxide form to oxide [31].

2.3. Characterization

The change of CFF color from colorless to white was monitored by measuring their absorbance using UV-Vis spectroscopy (JENWAY-6305) to detect the maximum Surface Plasmon Resonance (SPR) of synthesized MgO-NPs. The absorbance was measured in the range of 200 – 600 nm. The activity of different functional groups in CFF in the reduction, capping, and stabilizing of metal oxide to form nanostructure was investigated by Fourier transform infrared (FT-IR) spectroscopy (Agilent system Cary 660). Approximately, 50 mg of synthesized powder was mixed with KBr under high pressure to form a disk before being scanned at a wavenumber in the ranges of 400 – 4000 cm^{-1}[32-34].

The shape and size of probiotic-mediated green synthesis of MgO-NPs were detected by Transmission Electron Microscopy (TEM). The MgO-NPs powder was dissolved in high-purity H_2O (milli-Q) and a few drops were added to the carbon-copper grid before being subjected to vacuum

desiccation to dryer the loaded sample on the grid. The loaded sample was analyzed using a TEM instrument (JEOL 1010) under an acceleration voltage of 120 KV and X40000. The chemical compositions of synthesized MgO-NPs were assessed by Energy Dispersive X-Ray (EDX) analysis (JEOL, JSM-6360LA, Japan). The crystal phase of bacterial synthesized MgO-NPs was investigated by X-ray diffraction (XRD, X'Pert PRO, Philips, Eindhoven, Netherlands) with current and voltage of 30 mA and 40 KV respectively, and CuKα as a source of X-ray radiation. The analysis was achieved at 2θ values in the ranges of 10° – 80° [35]. The crystal size of synthesized MgO-NPs was measured based on XRD spectra by Debye–Scherrer equation as follows [36]:

$$Crystal\ size = K\lambda/\beta cos\theta$$

Where K is a Debye–Scherrer constant (0.9), λ is the X-ray radiation wavelength (0.154 nm), β is half of the maximum intensity, and θ is the Bragg's diffraction angle.

2.4. Antifungal activity

2.4.1. Fungal used

The antifungal activity of bacterial synthesized MgO-NPs was investigated against different fungal strains designated as *Aspergillususstus* AM4, *Penicilliumcitrinum* AM5, *Penicilliumchrysogenum* AM11, *A. terreus* AM12, *P. citrinum* AM13, *P. citrinum* AZ8, *P. citrinum* AZ9, *A. niger*AZ11, *P. chrysogenum* AZ12, and *P. chrysogenum* AZ13. These fungal strains were isolated from the highly deteriorated historical manuscripts (paper and leather) namely "Musnad of Imam Muhammad bin-Idris al-Shafi'I." and "Kashf al-Ramz 'an Khabaya al-Kanz" dated back to 14th and 17th century respectively[37, 38]. These strains were identified based on cultural and microscopic examination, and molecular identification using ITS sequence analysis, and selected due to their high activity to produce various extracellular hydrolytic enzymes such as cellulase, amylase, gelatinase, and pectinase. Before the experiment, the fungal strain was inoculated on potato dextrose agar media and incubated for 6 days at 25 ±2°C to check the purity.

2.4.2. Antifungal activity

The spore suspension of each fungal strain was prepared by mixing of fungal spore with sterilized phosphate buffer (pH = 7) and adjusting the spore density at 10^7 spores per mL through counting using a cell counter chamber. Approximately, 30 µL of spore suspension was spread over the potato dextrose agar plate by sterilizing glass rods before being made wells (8 mm in their diameter) in each plat using a sterilized cork borer. Approximately, 100 µL of stock solution (300 µg mL^{-1}) was added to the prepared wells, kept in refrigerator for one hour, followed by incubation the loaded plates at 25 ±2°C for 72 h. The results were recorded as a diameter of clear zone formed around each well [39, 40]. The minimum inhibitory concentration (MIC) was detected as the lowest concentration of MgO-NPs that inhibit the fungal growth (formed clear zone). To determine the MIC value, different concentrations (200, 100, 50, and 25 µg mL^{-1}) of the synthesized MgO-NPs were prepared. Adding 100 µL of each concentration to the well prepared in inoculated plate and kept in refrigerator for one hour before being incubated at 25 ±2°C for 72 h. The MIC value was detected based on lowest concentration caused inhibition zone [41]. The activity of crude extract of probiotic bacteria and DMSO (solvent system) was investigated as a control. The experiment was achieved in triplicate.

2.5. Statistical analysis

Results were statistically analyzed using SPSS v18 (SPSS Inc., Chicago, IL, USA). Analysis of variance (ANOVA) test was used for multiple sample comparison followed by multiple comparisons Tukey's test.

3. Result and discussion

3.1. Characterizations

3.1.1. UV-Vis spectroscopy

The conversion of bacterial biomass filtrate from colorless to white color after mixing with metal precursor indicates the reduction of metal precursor and formation of MgO-NPs. The bio-reduction of Mg^{+2} to Mg^0 could be attributed to the electrons that are liberated from the reduction of NO_3^- to NO_2^- by metabolites that exist in biomass filtrate [42], and hence the color intensity is combined with the number of reduced Mg^{+2} ions. The intensity of the formed color was checked by measuring their absorbance at a varied wavelength (i.e. 200 – 600 nm) to detect the maximum Surface Plasmon Resonance (SPR). Herein, the presence of a single peak at 240 nm (Fig. 1) indicates the formation of MgO-NPs with smaller sizes. The presence of a single-SPR band at a wavelength below 300 nm refers to the successful formation of small sizes MgO-NPs as reported previously [43]. The UV-Vis spectroscopy in the current study was compatible with published literature about the green synthesis of MgO-NPs by various biological entities [31, 38, 44].

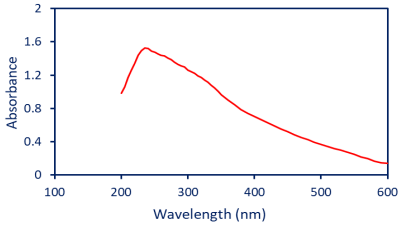

Fig. 1: The UV-vis spectroscopy of bacterial synthesized MgO-NPs showing the maximum SPR at 240 nm

3.1.2. Morphological and elemental analysis investigation (TEM, SAED, and EDX)

The activity of NPs is dependent on various factors such as shapes, sizes, surface area, surface charge, and agglomeration. TEM analysis is used to investigate the morphological characters of synthesized NPs including size, shape, and agglomeration. As shown, the metabolites of *L. gasseri* strain LA39 have the efficacy to fabricate spherical MgO-NPs with small sizes in the ranges of 1 – 10 nm (Fig. 2A). The obtained data are compatible with data of UV-Vis spectroscopy that predicted the formation of smaller size due to the SPR band at wavelength below 300 nm. The TEM image showed that the particles are coated with capping agents and arranged without aggregation. In a recent study, the aqueous extract of *Pterocarpusmarsupium* has the efficacy to green synthesized spherical MgO-NPs with sizes in the range of 10 – 20 nm [45]. Moreover, the biomass filtrate of the fungal strain *Aspergillusterreus* exhibit the potential to fabricate spherical MgO-NPs with sizes of 8 – 38 nm [46]. Also, the biomass filtrate of *Lactobacillus* sp. is used to synthesize MgO-NPs with spherical and oval shapes and sizes below 30 nm [31]. As mentioned, the activity of MgO-NPs was mainly depending on the sizes, the activity was increased at smaller sizes and vice versa. For instance, MgO-NPs with varied sizes of 35.9 nm, 47.3 nm, and 2145.9 nm (micron size) showed inhibitory effect toward *Bacillus subtilis* with percentages of 96%, 94%, and 75% respectively [47]. The SAED (selective area electron diffraction) pattern displayed the nanocrystalline nature of MgO-NPs and indexed thecubic phase (accordance with the XRD analysis) (Fig. 2B).

The elemental compositions of bacterial synthesized MgO-NPs were detected by Energy Dispersive X-Ray (EDX) analysis. Tabrez et al. reported that the quality and amount of production of NPs are correlated with the significant peaks that appear in the EDX analysis [43]. Figure 2C displayed the EDX spectrum of bacterial synthesized MgO-NPs with weight and atomic percentages of distinct peaks. As shown, the sample containing Mg and O in addition to other peaks for C, Na, and Cl. The Mg ion exhibited a maximum peak at bending energy in the ranges of 1.1 – 1.3 Kev followed by an O peak at bending energy of 0.5 KeV which confirmed the successful formation of MgO. Also, the weight and atomic percentages of Mg and O are represented by (42.3 and 36.92 %) and (39.07 and 38.7%) respectively. This means the Mg and O ions represented the maximum weight of the prepared sample. Compatible with the obtained results, the Mg and O represented the maximum weight of MgO-NPs fabricated by aqueous extract of *Saussureacostus* with percentages of 38.2 and 27.9% respectively [44]. The presence of other peaks (C, Na, and Cl) could be attributed to the scattering of capping agents such as proteins, carbohydrates, amino acids, and polysaccharides by X-ray [48]. These additional peaks were present with a small amount with weight and atomic percentages of (8.43, 11.21, and 1.14%) and (13.56, 8.05, and 0.62%) for C, Na, and Cl respectively (Fig. 2C).

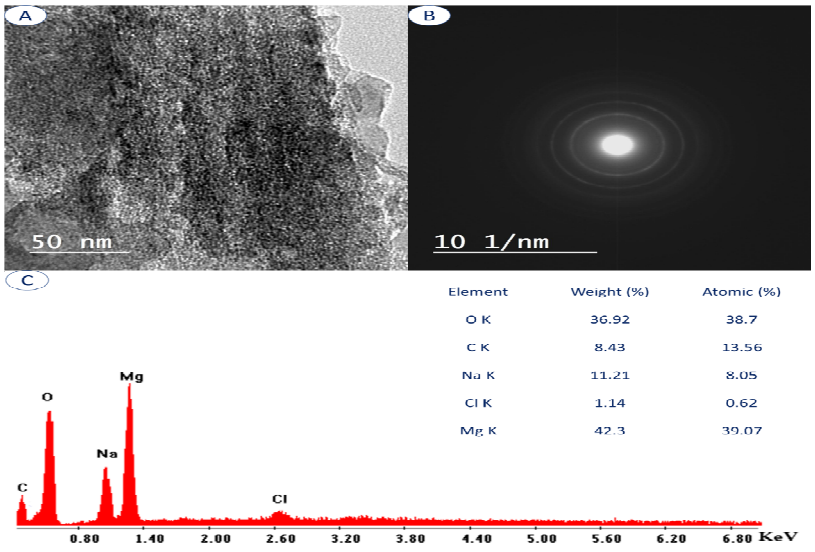

Fig. 2: Characterization of bacterial-mediated synthesis of MgO-NPs. A is TEM analysis showing a spherical shape; B is SAED, and C is EDX spectrum

3.1.3. Crystallinity nature assessment

The crystallographic structure of bacterial synthesized MgO-NPs was investigated by X-ray diffraction (XRD) pattern. Figure 3 showed that the XRD chart contains five diffraction peaks at two theta values of 36.8°, 42.9°, 62.3°, 75.8°, and 78.5° which correspond to planes of (111), (200), (220), (311), and (222) respectively. The obtained spectrum confirmed the crystalline nature of the face-centered cubic of bacterial synthesized MgO-NPs according to JCPDS standard with file number 89-4248 [43]. The presence of fine extra peaks indicates the presence of some impurities from capping agents (verified by EDX analysis). Based on XRD analysis, the prepared sample contained Mg $(OH)_2$ and MgO. The peaks at two theta values of 36.8° (111), 75.8° (311), and 78.5° (22) were referred to $Mg(OH)_2$ whereas peaks at two theta values of 42.9° (200) and 62.3° (220) corresponding to MgO[49, 50]. The crystallite size of synthesized MgO-NPs was detected based on XRD analysis using Debye–Scherrer equation which was less than 13 nm. The obtained data are matched with those reported that the crystallite size of face-cubic structure MgO-NPs detected by XRD was 13.3 nm [51]. Also, the crystallite size of phyto-synthesized MgO-NPs using an aqueous extract of *Swertiachirayaita* was less than 20 nm [52].

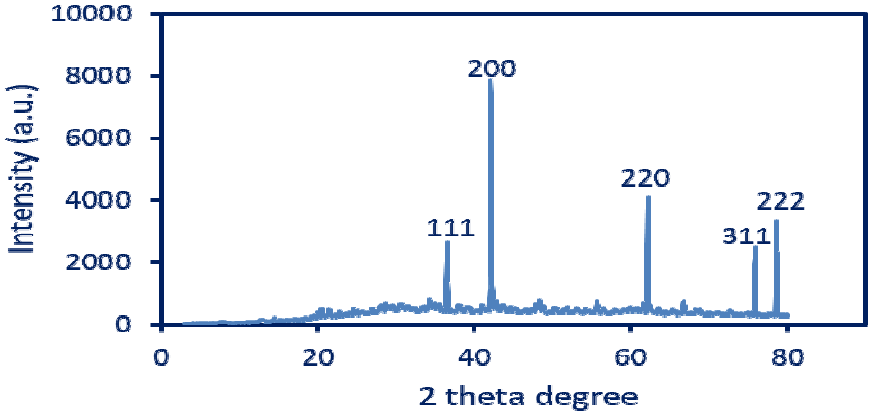

Fig. 3: X-ray diffraction of bacterial synthesized MgO-NPs showing crystalline nature

3.1.4. Fourier transform infrared (FT-IR) spectroscopy

The functional groups in biosynthesized MgO-NPs were assessed by FT-IR analysis. As shown, there are six peaks at wavenumbers 3355, 2360, 1640, 1350, 820, and 550 cm^{-1} (Fig. 4). The broadness peak at 3355 cm^{-1} signify to the N–H and O–H overlapping vibration [23, 53], whereas the peak at 2360 cm^{-1} corresponding to stretching C–H of methylene groups of proteins [54, 55]. The absorption peak at 1640 cm^{-1} is signifying the C═O, C═C, and N–H stretching of amide I, polysaccharide, and primary amine [56-58]. A peak at 1350 cm^{-1} is related to the stretching vibration of C–N of aromatic and aliphatic amines [27, 59]. The absorption peak at 820 cm^{-1} is corresponding to the bending vibration of N–H and ═C–H [60, 61]. The successful formation of Mg-O was confirmed by the peak at 550 cm^{-1} as reported previously [44, 49, 60]. As shown the presence of various bioactive molecules such as amine, proteins, amino acids, and polysaccharides have a crucial role in the bio-reduction, capping, and stabilizing of bacterial synthesized MgO-NPs.

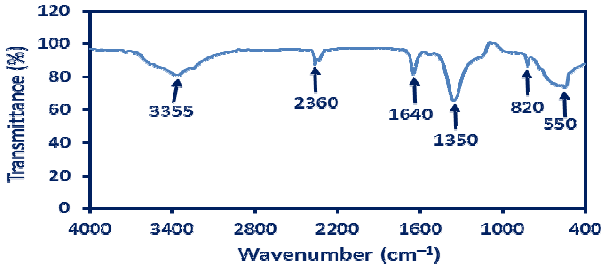

Fig. 4: FT-IR chart of MgO-NPs fabricated by biomass filtrate of *L. gasseri* strain LA39

3.2. Antifungal activity.

The activity of *L.gasseri*-mediated green synthesis of MgO-NPs versus the crude extract of probiotic bacterial strain was investigated against varied fungal strains. *Aspergillususstus* AM4, *Penicilliumcitrinum* AM5, *Penicilliumchrysogenum* AM11, *A. terreus* AM12, *P. citrinum* AM13, *P. citrinum* AZ8, *P. citrinum* AZ9, *A. niger*AZ11, *P. chrysogenum* AZ12, and *P. chrysogenum* AZ13 were selected based on their high activity to deteriorate the historical manuscript through secretion of different hydrolytic enzymes. As shown, the different concentrations (300, 200, 100, and 50 µg mL^{-1}) of green synthesized MgO-NPs have the efficacy to inhibit the growth of fungal strains in a dose-dependent manner (Fig. 5). This finding was in agreement with those reported that the activity of green synthesized NPs against fungal strains was dependent on the concentrations [62, 63]. The negative control (DMSO as solvent system) does not exhibit any activity, whereas crude extract (positive control) of probiotic bacterial strain has the potential to inhibit the fungal growth with low activity compared to MgO-NPs. The maximum clear zone formed due to treatment with crude extract was recorded against fungal strain *P. citrinum* AZ9 with a diameter of 16.7 ± 1.5 mm compared to the diameter of clear zones formed due to treatment with 300, 200, 100, 50 µg mL^{-1} of MgO-NPs which were 28.0 ± 1.0, 20.7 ± 0.6, 16.7 ± 0.7, and 13.7 ± 0.6 mm respectively (Fig. 5). The maximum inhibition zones were recorded for the highest MgO-NPs concentration (300 µg mL^{-1}) that recorded for fungal strains AM5 and AM11 with zone of inhibition of 27.7 ± 0.6 mm and 27.0 ± 1.0 mm respectively. In a similar study, the highest inhibition zones formed due to the treatment of *Aspergillusniger, Mucorplumbeus, Trichotheciumroseum, Penicilliumexpansum,* bacterial and fungal strains. For example, *Bacillus subtilis*, *Penicilliumchrysogenum,* and*Aspergillusniger* were selected among various bacterial and fungal strains isolated from deteriorated historical manuscripts due to their high hydrolytic enzyme activities. The growth of these bacterial and fungal strains was inhibited due to treatment with nano-silver and nano-zinc oxide [19, 67]. The activity of NPs to integrate into biomedical and biotechnological applications depends on different factors including sizes, shapes, aggregation value, surface area to volume ratio, distribution, and surface charge [21, 68]. When compared to NPs with larger diameters, NPs with smaller sizes had higher antimicrobial activity, which may be because smaller NPs have a high surface area [69]. This conclusion can explain the activity of green synthesized MgO-NPs in the current study against various fungal strains due to their smaller sizes (1 – 10 nm) which enhance their penetration of cell walls.

Alternariaalternata, Rhizoctoniasolani, and *Penicilliumchrysogenum* with MgO-NPs were recorded at 500 µg mL^{-1} with diameters of 14.7 ± 0.6, 13.3 ± 0.6, 15.3 ±1.2, 12.0 ± 1.0, 16.3 ± 1.2, 14.3 ± 0.6, and 14.3 ± 0.6 mm respectively [64].

The activity of MgO-NPs was decreased by lowering the concentration to be in the ranges of 13.3 ± 0.6 to 19.0 ± 1.0 mm at a concentration of 100 µg mL^{-1}. In addition, the positive control (bacterial crude extract) showed maximum inhibition zones of 14.3 ± 0.6 mm toward fungal strain of AZ11 and lowest inhibition zone of 12.3 ± 0.6 mm against strain AM4. As shown, the highest sensitive fungal strain toward MgO-NPs was *Penicilliumcitrinum* AM5 followed by *Penicilliumchrysogenum* AM11, *P. citrinum* AZ9, and *A. niger*AZ11 based on formed inhibition zones.

The lowest MgO-NP concentrations that have the efficacy to form a clear zone are defined as Minimum Inhibitory Concentrations (MIC). From the industrial and biomedical overview, it is important to detect the MIC value for synthesized active compounds. Herein, the MIC value of MgO-NPs was 100 µg mL^{-1} for fungal strains AM4, AM12, AM13, AZ11, and AZ13 with a zone of inhibition in the ranges of 13.3 ± 0.6 – 16.3 ± 0.6 mm. Whereas, the MIC value for the remaining fungal strains (AM5, AM11, AZ8, AZ9, and AZ12) was 50 µg mL^{-1} with inhibition zones in the ranges of 12.3 ± 0.6 – 15.3 ± 1.2 mm (Fig. 5).

Recently, different metal and metal-oxides NPs especially those synthesized by green approaches are used as eco-friendly, rapid, and cost-effective agents to inhibit the growth of different fungal strains [64-66]. Moreover, due to the unique properties of nanoscale compounds over bulk materials, they can be used in the treatment of archeological manuscripts to overcome the deterioration caused by various

The inhibitory mechanisms of MgO-NPs could be related to their dissolving and releasing toxic ions, which was Mg^{+2}, and interaction with amino acids containing sulfur groups such as methionine and cysteine, ultimately impairing their function. In addition, these toxic ions can be reacting with proteins embedded in the cytoplasmic membrane and lead to dysfunction of selective permeability [70, 71]. Moreover, fungal growth can be inhibited by NPs by blocking the conidia germination. Also, the reaction of NPs with the mitochondrial membrane can lead to an increase in the transcription of some genes responsible for oxidative stress such as catalase, GPx, and SOD2 which enhance the production of Reactive Oxygen Species (ROS). The overproduction of ROS leads to damage of proteins, DNA, enzymes, amino acids, and other macromolecules in eukaryotic cells [28, 69].

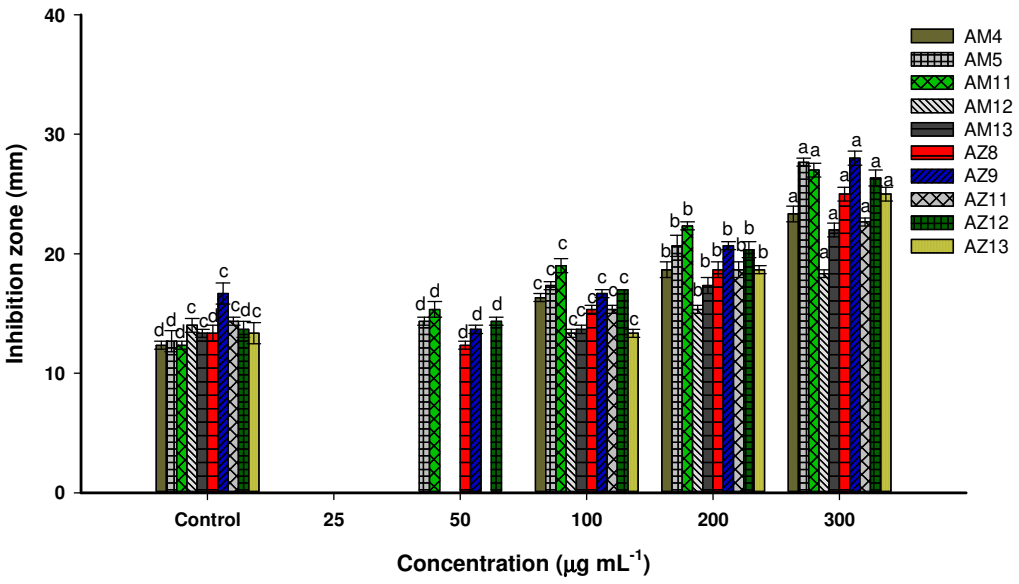

Fig. 5: Antifungal activity of green synthesized MgO-NPs at various concentrations (300, 200, 100, 50, and 25 µg mL^{-1}) versus crude extract of probiotic *L. gasseri* against highly deteriorated fungal strains isolated from historical manuscripts

4. Conclusion

Some highly deteriorated fungi isolated previously from some historical manuscripts and published before by the authors were used in this study. For the characterization of bacterial synthesized MgO-NPs, UV-Vis spectroscopy detected the presence of a single band for Surface Plasmon Resonance (SPR) of synthesized MgO-NPs) at a wavelength below 300 nm referred to its formation with small sizes in the ranges between 1 – 10 nm, and with a spherical shape, as was shown by TEM analysis. XRD analysis proved the nanocrystalline nature of MgO-NPs and indexed the cubic phase. EDX spectrum of bacterial synthesized MgO-NPs showed that the sample contained Mg and O in addition to other elements (C, Na, and Cl). FTIR analysis showed that the formation of Mg-O was confirmed by the peak at 550 cm^{-1}, and the presence of amine, proteins, amino acids, and polysaccharides as bioactive molecules have an important role in the bio-reduction, capping, and stabilizing of bacterial synthesized MgO-NPs. Different concentrations (300, 200, 100, and 50 µg mL^{-1}) of green synthesized MgO-NPs have different levels of efficacy to inhibit the growth of fungal strains depending on the concentration used. The inhibition zones increased with increasing the concentration of MgO-NPs. Accordingly, the maximum inhibition zone was obtained from the highest MgO-NPs concentration (300 µg mL^{-1}). The efficiency of the crude extract (positive control) of probiotic bacterial strain has the potential to inhibit the fungal growth more than MgO-NPs.

5. Acknowledgments: The authors extend their appreciation to the Botany and Microbiology Department, Faculty of Science, Al-Azhar University, Cairo, Egypt; Conservation Department, Faculty of Archaeology, Cairo University, Giza, Egypt; Department of Manuscripts Conservation, Al-Azhar Al-Sharif Library, Cairo, Egypt; and Food Toxicology and Contaminants Department, National Research Centre, Cairo, Egypt for the great support and cooperation in the achievement and publication of this research work.

6. References

1. Pinzari, F. and B. Gutarowska, *Extreme Colonizers and Rapid Profiteers: The Challenging World of Microorganisms That Attack Paper and Parchment*, in *Microorganisms in the Deterioration and Preservation of Cultural Heritage*, E. Joseph, Editor. 2021, Springer International Publishing: Cham. p. 79-113.
2. Saada, N.S., et al., *Evaluation and utilization of lemongrass oil nanoemulsion for disinfection of documentary heritage based on parchment.* Biocatalysis and Agricultural Biotechnology, 2020. **29**: p. 101839.

3. Abdel-Maksoud, G., M. Abdel-Hamied, and A.A. Abdelhafez, *Evaluation of the condition of a Mamluk-illuminated paper manuscript at Al-Azhar Library, Egypt.* Pigment & Resin Technology, 2021. **52**(1): p. 49-59.
4. Abdel-Nasser, M., et al. *Antifungal Activity of Cell-Free Filtrate of Probiotic Bacteria Lactobacillus rhamnosus ATCC-7469 against Fungal Strains Isolated from a Historical Manuscript*. Microorganisms, 2023. **11**, DOI: 10.3390/microorganisms11051104.
5. Kirtzel, J., et al., *Organic acids, siderophores, enzymes and mechanical pressure for black slate bioweathering with the basidiomycete Schizophyllum commune*. Environ Microbiol, 2020. **22**(4): p. 1535-1546.
6. Ismail, M.A., et al., *Comparative Study between Exogenously Applied Plant Growth Hormones versus Metabolites of Microbial Endophytes as Plant Growth-Promoting for Phaseolus vulgaris L.* Cells, 2021. **10**(5).
7. Abdel-Maksoud, G. and E. Marcinkowska, *Effect of artificial heat ageing on the humidity sorption of parchment and leathers compared with archaeological samples.* Journal of the Society of Leather Technologists and Chemists, 2000. **84**(5): p. 219-22.
8. Pinzari, F., et al., *Electronic Nose for the Early Detection of Moulds in Libraries and Archives.* Indoor and Built Environment - INDOOR BUILT ENVIRON, 2004. **13**: p. 387-395.
9. Salem, S.S., et al., *Biological Decolorization and Degradation of Azo Dyes from Textile Wastewater Effluent by Aspergillus niger.* Egyptian Journal of Chemistry, 2019. **62**(10): p. 1799-1813.
10. Nitiu, D.S., A.C. Mallo, and M.C.N. Saparrat, *Fungal melanins that deteriorate paper cultural heritage: An overview.* Mycologia, 2020. **112**(5): p. 859-870.
11. Abdel-Maksoud, G., et al., *Eco-friendly approach for control of fungal deterioration of archaeological skeleton dated back to the Greco-Roman period.* Journal of Cultural Heritage, 2023. **59**: p. 38-48.
12. Fouda, A., et al. *The Efficacy of Silver Nitrate (AgNO3) as a Coating Agent to Protect Paper against High Deteriorating Microbes*. Catalysts, 2021. **11**, DOI: 10.3390/catal11030310.
13. Abdel-Maksoud, G., *Evaluation of wax or oil/fungicide formulations for preservation of vegetable-tanned leather artifacts.* Journal of the Society of Leather Technologists and Chemists, 2006. **90**(2): p. 58-67.
14. Abdel-Maksoud, G., *Investigation techniques and conservation methods for a historical parchment document.* Journal of the Society of Leather Technologists and Chemists, 2011. **95**(1): p. 23-34.
15. Abdel-Maksoud, G. and A. El-Sayed, *Microscopic investigation for condition assessment of archaeological bones from different sites in Egypt* International Journal of Conservation Science, 2016. **7**(2).
16. Mesquita, N., et al., *Fungal diversity in ancient documents. A case study on the Archive of the University of Coimbra.* International Biodeterioration & Biodegradation, 2009. **63**(5): p. 626-629.
17. Crook, B. and N.C. Burton, *Indoor moulds, Sick Building Syndrome and building related illness.* Fungal Biology Reviews, 2010. **24**(3): p. 106-113.
18. Abdel-Maksoud, G., M. Abdel-Hamied, and A.A. Abdelhafez, *Condition Assessment of a Mamluk HistoricalIlluminated Leather Binding at the Libraryof Mashiakht El-Azhar, Egypt.* Journal of the Society of Leather Technologists and Chemists, 2021. **105**(5): p. 248-256.
19. Fouda, A., et al., *Eco-friendly approach utilizing green synthesized nanoparticles for paper conservation against microbes involved in biodeterioration of archaeological manuscript.* International Biodeterioration & Biodegradation, 2019. **142**: p. 160-169.
20. Hamza, M.F., et al., *Functionalization of magnetic chitosan microparticles for high-performance removal of chromate from aqueous solutions and tannery effluent.* Chemical Engineering Journal, 2022. **428**: p. 131775.
21. Huston, M., et al., *Green Synthesis of Nanomaterials.* Nanomaterials (Basel), 2021. **11**(8).
22. Nam, N.H. and N.H. Luong, *Nanoparticles: synthesis and applications; Materials for Biomedical Engineering.*, ed. V. Grumezescu and A.M. Grumezescu. 2019: doi: 10.1016/B978-0-08-102814-8.00008-1. Epub 2019 Mar 29. 211-40.
23. Hamza, M.F., et al. *High-Performance Hydrogel Based on Modified Chitosan for Removal of Heavy Metal Ions in Borehole: A Case Study from the Bahariya Oasis, Egypt*. Catalysts, 2022. **12**, DOI: 10.3390/catal12070721.
24. El-Naggar, M.E., et al., *Preparation of bactericidal zinc oxide nanoparticles loaded carboxymethyl cellulose/polyethylene glycol cryogel for gap filling of archaeological bones.*

Journal of Materials Research and Technology, 2022. **20**: p. 114-127.
25. Abdel-Nasser, M., et al., *Evaluation of the efficiency of nanoparticles for increasing α-amylase enzyme activity for removing starch stain from paper artifacts.* Journal of Cultural Heritage, 2022. **53**: p. 14-23.
26. He, Y., et al., *Study on the mechanism of antibacterial action of magnesium oxide nanoparticles against foodborne pathogens.* Journal of Nanobiotechnology, 2016. **14**(1): p. 54.
27. Dobrucka, R., *Synthesis of MgO Nanoparticles Using Artemisia abrotanum Herba Extract and Their Antioxidant and Photocatalytic Properties.* Iranian Journal of Science and Technology, Transactions A: Science, 2018. **42**(2): p. 547-555.
28. Venkatappa, M.M., et al. *Effect of Biofunctional Green Synthesized MgO-Nanoparticles on Oxidative-Stress-Induced Tissue Damage and Thrombosis*. Molecules, 2022. **27**, DOI: 10.3390/molecules27165162.
29. Ramos-Coria, D., et al., *Lactobacillus gasseri liver abscess and bacteremia: a case report.* BMC Infectious Diseases, 2021. **21**(1): p. 518.
30. Varela-Pérez, A., et al. *Encapsulation of Lactobacillus gasseri: Characterization, Probiotic Survival, In Vitro Evaluation and Viability in Apple Juice*. Foods, 2022. **11**, DOI: 10.3390/foods11050740.
31. Mohanasrinivasan, V., et al., *Biosynthesis of MgO Nanoparticles Using Lactobacillus Sp. and its Activity Against Human Leukemia Cell Lines HL-60.* BioNanoScience, 2018. **8**(1): p. 249-253.
32. Fouda, A., et al., *Antimicrobial, Antiviral, and In-Vitro Cytotoxicity and Mosquitocidal Activities of Portulaca oleracea-Based Green Synthesis of Selenium Nanoparticles.* J Funct Biomater, 2022. **13**(3).
33. Abdel-Maksoud, G., M. Abdel-Hamied, and H.A. El-Shemy, *Analytical techniques used for condition assessment of a late period mummy.* Journal of Cultural Heritage, 2021. **48**: p. 83-92.
34. Abdel-Maksoud, G., E.E. Abed al-Sameh Al-Shazly, and A.-R. El-Amin, *Damage caused by insects during the mummification process: an experimental study.* Archaeological and Anthropological Sciences, 2011. **3**: p. 291-308.
35. Abdel-Maksoud, G. and A. El-Sayed, *Analysis of archaeological bones from different sites in Egypt by a multiple techniques (XRD, EDX, FTIR).* Mediterr. Archaeol. Archaeom, 2016. **16**(2): p. 149-158.
36. Holzwarth, U. and N. Gibson, *The Scherrer equation versus the 'Debye-Scherrer equation'.* Nature Nanotechnology, 2011. **6**(9): p. 534-534.
37. Abdel-Maksoud, G., et al. *Fungal Biodeterioration of a Historical Manuscript Dating Back to the 14th Century: An Insight into Various Fungal Strains and Their Enzymatic Activities*. Life, 2022. **12**, DOI: 10.3390/life12111821.
38. Fouda, A., et al., *Investigate the role of fungal communities associated with a historical manuscript from the 17th century in biodegradation.* npj Materials Degradation, 2022. **6**(1): p. 88.
39. Balouiri, M., M. Sadiki, and S.K. Ibnsouda, *Methods for in vitro evaluating antimicrobial activity: A review.* J Pharm Anal, 2016. **6**(2): p. 71-79.
40. Fouda, A., et al. *Aspergillus flavus-Mediated Green Synthesis of Silver Nanoparticles and Evaluation of Their Antibacterial, Anti-Candida, Acaricides, and Photocatalytic Activities*. Catalysts, 2022. **12**, DOI: 10.3390/catal12050462.
41. Fouda, A., et al., *Light enhanced the antimicrobial, anticancer, and catalytic activities of selenium nanoparticles fabricated by endophytic fungal strain, Penicillium crustosum EP-1.* Scientific Reports, 2022. **12**(1): p. 11834.
42. Fouda, A., et al., *Photocatalytic degradation of real textile and tannery effluent using biosynthesized magnesium oxide nanoparticles (MgO-NPs), heavy metal adsorption, phytotoxicity, and antimicrobial activity.* Journal of Environmental Chemical Engineering, 2021. **9**(4): p. 105346.
43. Tabrez, S., et al., *Investigating the anticancer efficacy of biogenic synthesized MgONPs: An in vitro analysis.* Frontiers in Chemistry, 2022. **10**.
44. Amina, M., et al., *Biogenic green synthesis of MgO nanoparticles using Saussurea costus biomasses for a comprehensive detection of their antimicrobial, cytotoxicity against MCF-7 breast cancer cells and photocatalysis potentials.* PLoS One, 2020. **15**(8): p. e0237567.
45. Ammulu, M.A., et al., *Phytoassisted synthesis of magnesium oxide nanoparticles from Pterocarpus marsupium rox.b heartwood extract and its biomedical applications.* Journal of Genetic Engineering and Biotechnology, 2021. **19**(1): p. 21.
46. Saied, E., et al. *The Catalytic Activity of Biosynthesized Magnesium Oxide Nanoparticles (MgO-NPs) for Inhibiting the Growth of Pathogenic Microbes, Tanning Effluent Treatment, and Chromium Ion Removal*. Catalysts, 2021. **11**, DOI: 10.3390/catal11070821.

47. Huang, L., et al., *Influence of nano-MgO particle size on bactericidal action againstBacillus subtilis var. niger.* Chinese Science Bulletin, 2005. **50**(6): p. 514-519.
48. Hassan, S.E., et al., *Rhizopus oryzae-Mediated Green Synthesis of Magnesium Oxide Nanoparticles (MgO-NPs): A Promising Tool for Antimicrobial, Mosquitocidal Action, and Tanning Effluent Treatment.* J Fungi (Basel), 2021. **7**(5).
49. Nguyen, D.T.C., et al., *Biogenic synthesis of MgO nanoparticles from different extracts (flower, bark, leaf) of Tecoma stans (L.) and their utilization in selected organic dyes treatment.* Journal of Hazardous Materials, 2021. **404**: p. 124146.
50. Fouda, A., et al. *An Eco-Friendly Approach to the Control of Pathogenic Microbes and Anopheles stephensi Malarial Vector Using Magnesium Oxide Nanoparticles (Mg-NPs) Fabricated by Penicillium chrysogenum*. International Journal of Molecular Sciences, 2021. **22**, DOI: 10.3390/ijms22105096.
51. Sundrarajan, M., J. Suresh, and R. Gandhi, *A comparative study on antibacterial properties of MgO Nanoparticles prepared under different calcination temperature.* Digest J Nanomaterials Biostructures, 2012. **7**.
52. Sharma, G., R. Soni, and N.D. Jasuja, *Phytoassisted synthesis of magnesium oxide nanoparticles with Swertia chirayaita.* Journal of Taibah University for Science, 2017. **11**(3): p. 471-477.
53. Hamza, M.F., et al., *Phosphorylation of Guar Gum/Magnetite/Chitosan Nanocomposites for Uranium (VI) Sorption and Antibacterial Applications.* Molecules, 2021. **26**(7).
54. Coates, J., *Interpretation of Infrared Spectra, A Practical Approach*, in *Encyclopedia of Analytical Chemistry*. 2006.
55. Hamza, M.F., et al. *Photocatalytic Efficacy of Heterocyclic Base Grafted Chitosan Magnetite Nanoparticles on Sorption of Pb(II); Application on Mining Effluent*. Catalysts, 2022. **12**, DOI: 10.3390/catal12030330.
56. Ogunyemi, S.O., et al., *The Bio-Synthesis of Three Metal Oxide Nanoparticles (ZnO, MnO2, and MgO) and Their Antibacterial Activity Against the Bacterial Leaf Blight Pathogen.* Frontiers in Microbiology, 2020. **11**.
57. Hamza, M.F., et al., *Enhancement of Cerium Sorption onto Urea-Functionalized Magnetite Chitosan Microparticles by Sorbent Sulfonation-Application to Ore Leachate.* Molecules, 2022. **27**(21).
58. Hamza, M.F., et al., *Ecofriendly Composite as a Promising Material for Highly-Performance Uranium Recovery from Different Solutions.* Toxics, 2022. **10**(9).
59. Zahra, M.H., et al. *Synthesis of a Novel Adsorbent Based on Chitosan Magnetite Nanoparticles for the High Sorption of Cr (VI) Ions: A Study of Photocatalysis and Recovery on Tannery Effluents*. Catalysts, 2022. **12**, DOI: 10.3390/catal12070678.
60. Pugazhendhi, A., et al., *Anticancer, antimicrobial and photocatalytic activities of green synthesized magnesium oxide nanoparticles (MgONPs) using aqueous extract of Sargassum wightii.* Journal of Photochemistry and Photobiology B: Biology, 2019. **190**: p. 86-97.
61. Hamza, M.F., et al., *Poly-condensation of N-(2-acetamido)-2-aminoethanesulfonic acid with formaldehyde for the synthesis of a highly efficient sorbent for Cs(I).* Chemical Engineering Journal, 2023. **454**: p. 140155.
62. Hamza, M.F., et al., *Functionalized biobased composite for metal decontamination – Insight on uranium and application to water samples collected from wells in mining areas (Sinai, Egypt).* Chemical Engineering Journal, 2022. **431**: p. 133967.
63. Chen, J., et al., *Comparative Study on the Fungicidal Activity of Metallic MgO Nanoparticles and Macroscale MgO Against Soilborne Fungal Phytopathogens.* Frontiers in Microbiology, 2020. **11**.
64. Koka, J.A., A.H. Wani, and M.Y. Bhat, *Evaluation of antifungal activity of Magnesium oxide (MgO) and Iron oxide (FeO) nanoparticles on rot causing fungi.* Journal of Drug Delivery and Therapeutics, 2019. **9**(2-s): p. 173-178.
65. Bernardo-Mazariegos, E., et al., *Silver nanoparticles from Justicia spicigera and their antimicrobial potentialities in the biocontrol of foodborne bacteria and phytopathogenic fungi.* Rev Argent Microbiol, 2019. **51**(2): p. 103-109.
66. Hassan, S.E.-D., et al., *New approach for antimicrobial activity and bio-control of various pathogens by biosynthesized copper nanoparticles using endophytic actinomycetes.* Journal of Radiation Research and Applied Sciences, 2018. **11**(3): p. 262-270.
67. Fouda, A., et al., *Monitoring the effect of biosynthesized nanoparticles against biodeterioration of cellulose-based materials by Aspergillus niger.* Cellulose, 2019. **26**(11): p. 6583-6597.
68. Salem, S.S. and A. Fouda, *Green Synthesis of Metallic Nanoparticles and Their Prospective*

Biotechnological Applications: an Overview. Biol Trace Elem Res, 2021. **199**(1): p. 344-370.
69. Rai, M., et al., *Effective management of soft rot of ginger caused by Pythium spp. and Fusarium spp.: emerging role of nanotechnology*. Applied Microbiology and Biotechnology, 2018. **102**(16): p. 6827-6839.
70. Cruz-Luna, A.R., et al. *Metal Nanoparticles as Novel Antifungal Agents for Sustainable Agriculture: Current Advances and Future Directions*. Journal of Fungi, 2021. **7**, DOI: 10.3390/jof7121033.
71. Abdo, A.M., et al., *Green Synthesis of Zinc Oxide Nanoparticles (ZnO-NPs) by Pseudomonas aeruginosa and Their Activity against Pathogenic Microbes and Common House Mosquito, Culex pipiens.* Materials (Basel), 2021. **14**(22).